



**This document must be cited according to its final version
which is published in a journal as:**
P. Dufour¹, F. Couenne¹, Y. Touré²,
"Model predictive control of a catalytic reverse flow reactor",
IEEE Transactions on Control Systems Technology (TCST), special issue on
Control of Industrial Spatially Distributed Parameter Processes,
ISSN: 1063-6536
11(5), pp. 705-714, 2003.
<http://dx.doi.org/10.1109/TCST.2003.816408>

All open archive documents of Pascal Dufour are available at:
<http://hal.archives-ouvertes.fr/DUFOUR-PASCAL-C-3926-2008>

The professional web page (Fr/En) of Pascal Dufour is:
<http://www.lagep.univ-lyon1.fr/signatures/dufour.pascal>

1

Université de Lyon, Lyon, F-69003, France; Université Lyon 1;
CNRS UMR 5007 LAGEP (Laboratoire d'Automatique et de Génie des Procédés),
43 bd du 11 novembre, 69100 Villeurbanne, France
Tel +33 (0) 4 72 43 18 45 - Fax +33 (0) 4 72 43 16 99
<http://www-lagep.univ-lyon1.fr/> <http://www.univ-lyon1.fr> <http://www.cnrs.fr>

2

Université d'Orléans,
UPRES EA 2078 LVR (Laboratoire de Vision et de Robotique),
63 Av de Lattre de Tassigny, 18020 Bourges Cedex, France
<http://www.bourges.univ-orleans.fr/rech/lvr/>

Model Predictive Control of a Catalytic Reverse

Flow Reactor

Pascal Dufour¹, Françoise Couenne¹, Youssefi Touré²

¹ LAGEP UMR 5007 CNRS, University Claude Bernard Lyon 1

43 bd du 11 Novembre 1918

69622 Villeurbanne Cedex, France

² LVR UPRES EA 2078, University of Orléans

63 avenue de Lattre de Tassigny

18020 Bourges Cedex, France

Abstract

This paper deals with the control of a catalytic reverse flow reactor. The aim of this process is to reduce, by catalytic reaction, the amount of volatile organic compounds (VOCs) released in the atmosphere. The peculiarity of this process is that the gas flow inside the reactor is periodically reversed in order to trap the heat released during the reaction inside the process. This allows use of the reactor in heat saving mode. The goal of this work is to provide a model predictive control (MPC) framework to significantly enhance the poor overall performance currently obtained through the actual control strategy. It is directly addressed for the nonlinear parabolic partial differential equations (PDEs) that describe the catalytic reverse flow reactor. In the context of the application of MPC to this particular distributed parameter system, we propose a method that aims to reduce the on-line computation time needed by the control algorithm. The nonlinear model is linearized around a given operating trajectory to obtain the model to be solved on-line in the approach. MPC strategy combined with internal model control (IMC) structure allows to use less accurate and less time consuming control algorithm. The efficiency of the method is shown in simulation for this SISO system.

Keywords

Reverse flow reactor, VOC combustion, nonlinear distributed parameter system, MPC, IMC, modeling.

Corresponding author: dufour@lagep.univ-lyon1.fr, Phone: +33 4 72 43 18 78, Fax: +33 4 72 43 16 99.

Problems of environment pollution due to the industrial production are receiving increased attention. Due to public regulations, VOCs discharge in the atmosphere is strictly limited. Even if the definition of VOCs is blurred, it includes noxious products which chemical reactivity is likely to influence atmospheric pollution. For this reason, they are the source of a lot of environmental problems including: acid rains, woods wasting, greenhouse effect and health troubles. Therefore, the VOCs emission reduction represents a priority, especially since the problem is connected with a large field of activities from large-scale factories to small and medium-sized firms like dry cleaners. An experimental process was build-up in the LGPC ¹. It is a reverse flow reactor (RFR) that allows high temperatures in catalyst bed whereas the inlet and outlet gas stream temperatures are close to ambient temperature. This process is useful for experimental validation of solution for issues like: physical phenomena that influence purification efficiency, optimal size of each elements, process behavior in industrial use and control.

The aim of this paper is to develop a model-based control strategy for this RFR based on its spatial description. Both modeling and control aspects are detailed. The paper is structured as follows: first, the experimental process of the LGPC is presented. The catalytic reaction in the RFR is detailed through a first-principles model described by a nonlinear distributed parameter system and the related control problem is stated. Control of the process is addressed using a model-based predictive control framework with the internal model control structure. Technical aspects of the control strategy are detailed. Validity of the approach is demonstrated using simulation.

II. DESTRUCTION OF VOCs WITH THE RFR

The peculiarity of this process is that the gas circulation sense is periodically reversed (Fig. 1). The operation procedure of this RFR [1] is described below:

¹Laboratoire de Génie des Procédés Catalytiques, UMR CNRS 2214, CPE Lyon, France.

• A semi-cycle begins as follows: the gas flows through the first thermal monolith. It is made up of cordierite and of nb_c canals where the gas flows. The shape of its section is a nest (Fig. 2). The increase of gas temperature in the canals is due to the heat exchange with the cordierite. No reaction takes place;

• The gas then passes through the first catalytic monolith. This one is like the first thermal monolith but with catalytic elements (platinum and other noble metals) layers on the canals surface. With these elements, the exothermic chemical reaction takes place, inducing the increase of temperature in the cordierite and a concentration drop for the VOCs;

• The gas flows now in the empty central zone where control of a electrical heat source is provided, allowing control of the reaction;

• The reaction continues in a second catalytic monolith and finally the gas reaches a second thermal monolith where no reaction occurs but where the heat of reaction is exchanged from the gas to the cordierite.

• At the end of this semi-cycle, the flow rate inside the monoliths is reversed by the switch of the four servovalves. A second semi-cycle, identical to the first one, starts but in the reverse circulation sense;

• Since the circulation sense has changed, the polluted gas passes first through the previous second thermal monolith. In this zone, the gas temperature increases using the heat previously accumulated in the monolith during the first semi-cycle: This is the saving mode of the process;

• At the end of this second semi-cycle, the flow rate in the reactor is again reversed thanks to the servovalves switch and a new complete cycle begins.

According to the operating conditions, various problematic behaviors can take place:

• Unsuccessfully polluted gas causes, by its low heat release during the reaction, the extinction of the reactor if no external heat is supplied;

• With a strongly polluted gas, the release of heat due to the reaction can deteriorate the monolith.

To overcome extinction and overheating, several technical solutions have been proposed [2]:

- Extinction: fuel addition in the gas or energy addition in the central zone.
- Overheating: use of a bypass to redirect some amount of the gas or injection of cold gas in the central zone.

In this paper, we consider a SISO problem for the extinction problem where the technological solution adopted is a electric power supply in the central zone.

III. MODELING

VOCs combustion in a RFR has been studied in packed bed or monolith by various authors (see [1] for a general review). Models are based on standard heat and mass balances and most often deal with an adiabatic RFR at stationary periodic state [3], [4], [5]. They assume the analogy with a counter current reactor for the RFR at high frequency, which allows to estimate simple RFR characteristics. In [6], authors study the effects of an external electrical heater supply for very lean mixture. The dynamic aspects of the RFR have been less examined. In the LGPC, a simple linear dynamic model accounting for heat losses and dilution has been developed [7]. Budman *et al.* [8] have developed a nonlinear dynamic model. Quiet similar to this one, in our approach, one assumes that the adiabatic RFR has dynamic behavior, that gas velocity is constant and that there is no pressure loss. The heat and mass balances are described along the independent space variable z following the flow sense. Due to high thermal capacity and short residence time in the reactor, the phenomena in the canals are assumed instantaneous. In the solid parts, it is also assumed that the dynamic of the concentration is negligible with respect to the dynamic of the temperature. The following physical quantities are considered in each of the five zones (Fig. 3) of the reverse flow reactor (two thermal monoliths, two catalytic monoliths and the central part):

- The concentration $C_g(z, t)$ and the temperature $T_g(z, t)$ of the gas inside the canals;
- The concentration $C_s(z, t)$ and the temperature $T_s(z, t)$ in the cordierite along the solid parts.

Description and value of the model parameters are given in table 2, geometric data of the RFR are given in table 3.

Remark III.1: All the model parameters are constant except the gas characteristics at the process inlet: the concentration and the temperature.

To account for the periodic sense inversion, the model is written in four steps over a complete cycle $T =]\tau, \tau + T_{cycle}]$ where $\tau = nT_{cycle}$, (n is an integer).

1/ during the first semi-cycle ($t \in]\tau, \tau + \frac{T_{cycle}}{2}[$):

- at the inlet ($z = 0$):

$$\begin{cases} T_g = T_{g.inlet}(t) \\ C_g = C_{g.inlet}(t) \\ \frac{\partial T_s}{\partial z} = 0 \\ C_s = 0 \end{cases} \quad (1)$$

- in the first thermal zone (for $z \in \Omega_{MT1}$):

$$\begin{cases} \frac{\partial T_g}{\partial z} = \frac{h a_c}{u_g \rho_g c_{p_g}} (T_s - T_g) \\ C_g = C_g(0, t) \\ \frac{\partial T_s}{\partial t} = \frac{\lambda}{\rho_{st} c_{p_s}} \frac{\partial^2 T_s}{\partial z^2} + \frac{h a_c}{(1-\varepsilon) \rho_{st} c_{p_s}} (T_g - T_s) \\ C_s = 0 \end{cases} \quad (2)$$

- at the boundary between the first thermal zone and the first catalytic zone ($z = z_{MT1}$):

$$\begin{cases} T_g|_{z^-} = T_g|_{z^+} \\ C_g = C_g(0, t) \\ \frac{\partial T_s}{\partial z}|_{z^-} = \frac{\partial T_s}{\partial z}|_{z^+} \\ C_s = 0 \end{cases} \quad (3)$$

- in the first catalytic zone ($z \in \Omega_{MC1}$):

$$\begin{cases} \frac{\partial T_g}{\partial z} = \frac{h a_c}{u_g \rho_g c_{pg}} (T_s - T_g) \\ \frac{\partial C_g}{\partial z} = \frac{k_d a_c}{u_g} (C_s - C_g) \\ \frac{\partial T_s}{\partial t} = \frac{\lambda}{\rho_{sc} c_{ps}} \frac{\partial^2 T_s}{\partial z^2} + \frac{h a_c}{(1-\varepsilon) \rho_{st} c_{ps}} (T_g - T_s) + \frac{(-\Delta H_r) k^\infty a_c}{(1-\varepsilon) \rho_{sc} c_{ps}} e^{-\frac{E_a}{RT_s}} C_s \\ C_s = \frac{1}{1 + \frac{k^\infty}{k_d} e^{-\frac{E_a}{RT_s}}} C_g \end{cases} \quad (4)$$

- at the outlet of the first catalytic zone ($z = z_{MC1}$):

$$\begin{cases} \frac{\partial T_g}{\partial z} = \frac{h a_c}{u_g \rho_g c_{pg}} (T_s - T_g) \\ \frac{\partial C_g}{\partial z} = \frac{k_d a_c}{u_g} (C_s - C_g) \\ \frac{\partial T_s}{\partial z} = 0 \\ C_s = \frac{1}{1 + \frac{k^\infty}{k_d} e^{-\frac{E_a}{RT_s}}} C_g \end{cases} \quad (5)$$

- in the central zone (for $z \in \Omega_{ZC}$), the manipulated variable P_{res} is accounted for:

$$\begin{cases} \frac{\partial T_g}{\partial z} = \frac{1}{S u_g \rho_g c_{pg} L_{ZC}} P_{res} \\ C_g = C_g(z_{MC1}, t) \end{cases} \quad (6)$$

- at the central zone outlet ($z = z_{ZC}$):

$$\begin{cases} \frac{\partial T_g}{\partial z} = \frac{h a_c}{u_g \rho_g c_{pg}} (T_s - T_g) \\ \frac{\partial C_g}{\partial z} = \frac{k_d a_c}{u_g} (C_s - C_g) \\ \frac{\partial T_s}{\partial z} = 0 \\ C_s = \frac{1}{1 + \frac{k^\infty}{k_d} e^{-\frac{E_a}{RT_s}}} C_g \end{cases} \quad (7)$$

- in the second catalytic zone (for $z \in \Omega_{MC2}$):

$$\left\{ \begin{array}{l} \frac{\partial T_g}{\partial z} = \frac{h a_c}{u_g \rho_g c_{pg}} (T_s - T_g) \\ \frac{\partial C_g}{\partial z} = \frac{k_d a_c}{u_g} (C_s - C_g) \\ \frac{\partial T_s}{\partial t} = \frac{\lambda}{\rho_{sc} c_{ps}} \frac{\partial^2 T_s}{\partial z^2} + \frac{h a_c}{(1-\varepsilon) \rho_{st} c_{ps}} (T_g - T_s) + \frac{(-\Delta H_r) k^\infty a_c}{(1-\varepsilon) \rho_{sc} c_{ps}} e^{\frac{-E_a}{RT_s}} C_s \\ C_s = \frac{1}{1 + \frac{k^\infty}{k_d} e^{\frac{-E_a}{RT_s}}} C_g \end{array} \right. \quad (8)$$

- at the boundary between the second catalytic zone and the second thermal zone ($z = z_{MC2}$):

$$\left\{ \begin{array}{l} T_g|_{z^-} = T_g|_{z^+} \\ C_g = C_g(z_{MC2}, t) \\ \frac{\partial T_s}{\partial z}|_{z^-} = \frac{\partial T_s}{\partial z}|_{z^+} \\ C_s = \frac{1}{1 + \frac{k^\infty}{k_d} e^{\frac{-E_a}{RT_s}}} C_g \end{array} \right. \quad (9)$$

- in the second thermal zone (for $z \in \Omega_{MT2}$):

$$\left\{ \begin{array}{l} \frac{\partial T_g}{\partial z} = \frac{h a_c}{u_g \rho_g c_{pg}} (T_s - T_g) \\ C_g = C_g(z_{MC2}, t) \\ \frac{\partial T_s}{\partial t} = \frac{\lambda}{\rho_{st} c_{ps}} \frac{\partial^2 T_s}{\partial z^2} + \frac{h a_c}{(1-\varepsilon) \rho_{st} c_{ps}} (T_g - T_s) \\ C_s = 0 \end{array} \right. \quad (10)$$

- at the process outlet ($z = z_{MT2}$):

$$\left\{ \begin{array}{l} \frac{\partial T_g}{\partial z} = \frac{h a_c}{u_g \rho_g c_{pg}} (T_s - T_g) \\ C_g = C_g(z_{MC2}, t) \\ \frac{\partial T_s}{\partial z} = 0 \\ C_s = 0 \end{array} \right. \quad (11)$$

2/ At the end of the semi-cycle ($t = \tau + \frac{T_{cycle}}{2}$), the change of the circulation sense leads to a state permutation (L_{tot} is the total length of the reactor):

$$\begin{cases} T_g(z, \tau + \frac{T_{cycle}}{2}) = T_g(L_{tot} - z, \tau + \frac{T_{cycle}}{2}^-) \\ C_g(z, \tau + \frac{T_{cycle}}{2}) = C_g(L_{tot} - z, \tau + \frac{T_{cycle}}{2}^-) \\ T_s(z, \tau + \frac{T_{cycle}}{2}) = T_s(L_{tot} - z, \tau + \frac{T_{cycle}}{2}^-) \\ C_s(z, \tau + \frac{T_{cycle}}{2}) = C_s(L_{tot} - z, \tau + \frac{T_{cycle}}{2}^-) \end{cases} \quad (12)$$

3/ During the second semi-cycle ($t \in]\tau + \frac{T_{cycle}}{2}, \tau + T_{cycle}[$), equations (1) to (11) are again valid.

4/ At the end of the cycle ($t = \tau + T_{cycle}$), another state permutation takes place and a new complete cycle begins:

$$\begin{cases} T_g(z, \tau + T_{cycle}) = T_g(L_{tot} - z, \tau + T_{cycle}^-) \\ C_g(z, \tau + T_{cycle}) = C_g(L_{tot} - z, \tau + T_{cycle}^-) \\ T_s(z, \tau + T_{cycle}) = T_s(L_{tot} - z, \tau + T_{cycle}^-) \\ C_s(z, \tau + T_{cycle}) = C_s(L_{tot} - z, \tau + T_{cycle}^-) \end{cases} \quad (13)$$

The output is the mean output concentration calculated over a past time window T :

$$C_{g.outlet}(t) = \frac{1}{T} \int_{t-T}^t C_g(z_{MT2}, \tau) d\tau \quad (14)$$

The model clearly exhibits a nonlinear behavior due to catalytic reaction. For more details about the modeling, reader is referred to [7], [9]. Therefore, we consider the class of SISO one dimensional nonlinear parabolic PDEs with scalar control:

$$(S_{NL}) \begin{cases} \frac{\partial \underline{x}(z,t)}{\partial t} = F_d(\underline{x}(z,t), u(t), t) \quad \forall z \in \Omega, t > 0 \\ F_b(\underline{x}(z,t), t) = 0 \quad \forall z \in \partial\Omega, t > 0 \\ \underline{x}(z, 0) = \underline{x}_i \quad \forall z \in \Omega \cup \partial\Omega \\ y_m(t) = C(t)\underline{x}(z,t) \quad \forall z \in \partial\Omega, t > 0 \end{cases} \quad (15)$$

where z is the independent space variable, Ω is the spatial domain and $\partial\Omega$ its boundary, t is the independent time variable. \underline{x} is the state vector in a Hilbert Space, u is the control or manipulated variable (MV) in \mathbb{R} , y_m is the model output in \mathbb{R} . F_d and F_b are nonlinear operator [10]. C is a linear operator [11].

Assumption 1: There exists $u(t) = u_0(t)$ leading to the particular representation (S_0) of (S_{NL}) described by the triplet $\{u(t) = u_0(t), \underline{x}(z, t) = \underline{x}_0(z, t), y_m(t) = y_0(t)\}$.

Variations around (S_0) are given by:

$$\begin{cases} u(t) = u_0(t) + \Delta u(t) \\ \underline{x}(t) = \underline{x}_0(t) + \Delta \underline{x}(t) \\ y_m(t) = y_0(t) + \Delta y_m(t) \end{cases} \quad (16)$$

where sufficiently small variations are described by the time-varying linearized model (S_{LTV}) obtained about (S_0) :

$$(S_{LTV}) \begin{cases} \frac{\partial \Delta \underline{x}(z, t)}{\partial t} = A_d^x(t) \Delta \underline{x}(z, t) + A_d^u(t) u(t) & \forall z \in \Omega, t > 0 \\ A_b(t) \Delta \underline{x}(z, t) = 0 & \forall z \in \partial\Omega, t > 0 \\ \Delta \underline{x}(z, 0) = \underline{0} & \forall z \in \Omega \cup \partial\Omega \\ \Delta y_m(t) = C(t) \Delta \underline{x}(z, t) & \forall z \in \Omega \cup \partial\Omega, t > 0 \end{cases} \quad (17)$$

where the time-varying linear operators $A_d^x(t)$, $A_d^u(t)$ and $A_b(t)$ are obtained from the linearization of (S_{NL}) about the behavior described by (S_0) .

IV. CONTROL PROBLEM STATEMENT

Few papers are devoted to RFR control: [2] deals with this problem with ignition and extinction phenomena, whereas [12] gives some guidelines for the control of such process accounting for autothermal and overheating phenomena. Until now, the most complete control study has been written by Budman *et al.* [8] where a first-principles pseudo-homogeneous one-dimensional model is provided. A parametric study of the reactor is given that allows to characterize the working mode of the reactor

with respect to the two manipulated variables: the coolant flowrate and the cycle time. Moreover, Budman *et al.* developed two SISO control approaches (coolant flowrate is the MV) in the case where temperature and concentration at the reactor inlet were assumed constant. First, a PID controller, based on a local linear model is tuned, is given. Secondly, a feedforward controller is given but it is not usable during transient conditions and it is not robust with respect to modeling errors.

Compared with Budman *et al.*'s work, in our approach, the cycle time can not be chosen as a manipulated variable: indeed, the residence time of the gas inside the reactor has to be small (a few seconds) in order to trap the heat inside the reactor (for a complete discussion of the parametric study, the reader is referred to [7]). Cycle time is therefore constant and tuned to 20s. Moreover, simulation results cover here more realistic cases since gas concentration at the reactor inlet, i.e the input disturbance, is time-varying (which is not the case in Budman *et al.*'s work). The control problem for the RFR relates to the statutory maximum amount of VOC that can be released into the atmosphere at the process outlet. This is stated as a constraint: one has to ensure that the concentration of pollutant at the process outlet is lower than a maximum level fixed by public regulations:

$$C_g(z_{MT2}, t) \leq C_{g.\max} \quad (18)$$

From a practical point of view, it is replaced by a constraint on the mean output concentration calculated over a past time window T given Eq. (14):

$$C_{g.outlet}(t) \leq C_{g.\max} \quad (19)$$

Such a formulation permits possible VOCs overshoots. The existing control strategy deals with regulation of the temperature in the control zone Ω_{ZC} at $360^\circ C$. Indeed, according to practical analysis, this temperature setpoint allows to fulfill constraint (18) and therefore (19) is always checked. The drawback in this simple and easy to tune control strategy is that an overconsumption of electrical power fed in the central zone is imposed although it could be avoided. In our approach, we propose to formulate a better control objective in order to improve process use. Reminder of this paper is

devoted to the description of a model-based control strategy that leads to optimize the compromise between constraint (19) checking and a low consumption of electrical energy. Presence of constraints makes MPC well suited to solve this control problem.

V. MODEL PREDICTIVE CONTROL FORMULATION

MPC or receding horizon control refers to a class of control algorithms in which a dynamic process model is used to predict and optimize process performance. The idea is to solve, at each sample time, an open-loop optimization problem over a finite prediction horizon in order to find the value of the manipulated variable that has to be implemented. The procedure is reiterated at the next sample time with the update of process measurements. Today, MPC has become a control strategy widely used in industry. Indeed, MPC is well suited for high performance control since constraints can be explicitly incorporated into the formulation of the control problem. More details and references on MPC can be found in [13], [14], [15], [16]. From a practical point of view, one of the drawbacks of MPC is the computational time aspect, especially when the model becomes more complex and more accurate. Indeed, the model is intended to predict the future dynamic behavior of the process output over a finite prediction horizon and has to be solved during the on-line constrained optimization problem resolution. Reduction of this computational time is tackled in this section.

A. Discrete time MPC formulation

One of the advantages of MPC formulation as a constrained optimization problem is that a large number of control problems can be stated. It covers trajectory tracking for controlled variables (CVs), minimization of any economic function, minimization of energy supply under technical specifications, etc. Therefore, one can consider the following general task of minimizing, under some constraints, the cost function J (also named performance index):

$$\min_{\tilde{u}} J(\tilde{u}) = \sum_j g(y_p(j), u(j-1)) \quad \forall j \in J_1^{N_p} = \{k+1, \dots, k+N_p\} \quad (20)$$

where k is the actual discrete time index, j is the discrete time index, N_p is the receding horizon, $J_1^{N_p}$ is the future discrete time window, y_p is the process CV and \tilde{u} is the sought optimal sequence of the future MV u of the process that is classically tuned as follows:

$$\tilde{u} = [\dots u(j) \dots]^T \quad \forall j \in J_0^{N_c-1} = \{k, \dots, k + N_c - 1\} \quad (21)$$

where N_c is the control horizon and where:

$$u(j) = u(k + N_c - 1) \quad \forall j \in J_{N_c}^{N_p-1} = \{k + N_c, \dots, k + N_p - 1\} \quad (22)$$

This optimization problem has also to account for:

- constraints on the magnitude and velocity of the MV:

$$\begin{cases} u_{\min} \leq u(j) \leq u_{\max} & \forall j \in J_0^{N_p-1} = \{k, \dots, k + N_p - 1\} \\ \Delta u_{\min} \leq u(j) - u(j-1) \leq \Delta u_{\max} & \forall j \in J_0^{N_p-1} \end{cases} \quad (23)$$

- n general output constraints for the CV:

$$c_i(y_p(j), u(j-1)) \leq 0 \quad \forall j \in J_1^{N_p}, \quad \forall i \in I_1^n = \{1, \dots, n\} \quad (24)$$

In the performance index given in Eq. (20), one needs, at the current discrete time k , the value of the future measurements y_p over the prediction horizon N_p . This impossibility can be handled using the internal model control structure [17] in the MPC structure where the MV is applied to both the process and the model (Fig. 4). In our approach, the difference $e(j) = y_p(j) - y_m(j)$ between process and model CV and the model CV $y_m(j)$ are feedback into the controller. The latter feedback loop aims to correct modeling errors introduced in the model-based on-line optimizer [18].

Assumption 2: At each sample time k , the error $e(j)$ between the process output and the model output remains the same over the prediction horizon N_p . The error value is updated at each time k .

This assumption is classical [19], [17] and allows us to introduce the model (S_{NL}) into the constrained optimization problem and the feedback term $e(k)$ as well:

$$\left\{ \begin{array}{l} \min_{\tilde{u}} J(\tilde{u}) = \sum_{j \in J_1^{N_p}} g(y_m(j), u(j-1), e(k)) \\ \tilde{u} = [\dots u(j) \dots]^T \quad \forall j \in J_0^{N_c-1} \\ u(j) = u(k + N_c - 1) \quad \forall j \in J_{N_c}^{N_p-1} \\ u_{\min} \leq u(j) \leq u_{\max} \quad \forall j \in J_0^{N_p-1} \\ \Delta u_{\min} \leq u(j) - u(j-1) \leq \Delta u_{\max} \quad \forall j \in J_0^{N_p-1} \\ c_i(y_m(j), u(j-1), e(k)) \leq 0 \quad \forall j \in J_1^{N_p}, \forall i \in I_1^n \\ \text{and subject to the resolution of the model } (S_{NL}). \end{array} \right. \quad (25)$$

Remark V.1: $y_m(j)$ is the sampled value obtained from the resolution of the continuous model (S_{NL}).

B. Off-line and on-line IMC-MPC structures

On-line computational time is dealing with the resolution of the optimization problem that includes the model resolution. Discretization of the PDE model can lead to a large amount of algebraic differential equations that increases the computational burden, especially in the nonlinear case. In order to reduce the on-line computational time, the IMC-MPC structure is used off-line for the system (S_{NL}). As previously described, given small input variation Δu , small state variations $\Delta \underline{x}$ and small output variation Δy_m about (S_0) can be represented through the time-varying linearized model (S_{LTV}). Finally, the nominal nonlinear behavior (S_0) obtained off-line and the on-line time-varying linearized model (S_{LTV}) replace the initial nonlinear model (S_{NL}) in the IMC-MPC structure as depicted in Fig. 5. The control objective is then to find the variation Δu of the manipulated variable u about a chosen trajectory u_0 that improves at each sample time the on-line optimization result.

The next step developed is concerned with methods to handle constraints which aim to reduce the on-line optimization problem resolution time.

C. Constraints handling

Two different kinds of constraints are to be accounted for: constraints acting only on MV and constraints acting on CV.

C.1 Input constraints handling

Transformation method for variables allows to translate explicit constraints on the optimization argument u (and only the optimization argument) as new equations for a new unconstrained argument p . Here, we propose to enlarge this method to cover magnitude constraints and velocity constraints as well (acceleration rate constraints may also be accounted for). This leads to a transformation equation:

$$\begin{cases} u(j) = f(p(j)) = f_{\text{mean}} + f_{\text{magn}} \tanh\left(\frac{p(j) - f_{\text{mean}}}{f_{\text{magn}}}\right) & \forall j \in J_0^{N_c-1} \\ p(j) \in \mathbb{R} & \forall j \in J_0^{N_c-1} \end{cases} \quad (26)$$

with the time-varying coefficients f_{mean} and f_{magn} updated at each time k :

$$\begin{cases} f_{\text{mean}} = \frac{f_{\text{max}} + f_{\text{min}}}{2} \\ f_{\text{magn}} = \frac{f_{\text{max}} - f_{\text{min}}}{2} \\ f_{\text{min}} = \max(u_{\text{min}}, u(j-1) + \Delta u_{\text{min}}) & \forall j \in J_0^{N_c-1} \\ f_{\text{max}} = \min(u_{\text{max}}, u(j-1) + \Delta u_{\text{max}}) & \forall j \in J_0^{N_c-1} \end{cases} \quad (27)$$

C.2 Output constraints handling

In order to take account for output constraints, we adopt the exterior penalty method [20] used in nonlinear programming where a positive defined weighted penalty term is added to the initial cost function J :

$$\begin{cases} J_{\text{tot}} = J + J_{\text{ext}} \\ J_{\text{ext}} = \sum_{j \in J_1^{N_p}} \left(\sum_{i \in I_1^p} w_i \max^2(0, c_i) \right) \end{cases} \quad (28)$$

where w_i is an adaptive positive defined weight. The penalty method transforms the problem into an unconstrained problem by substituting a penalty function for the constraint. Solution of the resulting sequence of unconstrained problem tends to a constrained minimum.

D. Final penalized optimization problem

Finally, combining the transformation method for the constraints on the MV and the exterior penalty method for the constraints on the CV, the final penalized optimization problem to be solved on-line is the following one:

$$\left\{ \begin{array}{l} \min_{\Delta \tilde{p}} J_{tot}(\Delta \tilde{p}) = \sum_{j \in J_1^{N_p}} g(\Delta y_m(j), \Delta p(j-1), e(k)) + \\ \quad \sum_{j \in J_1^{N_p}} \left(\sum_{i \in I_1^n} w_i \max^2(0, c_i(\Delta y_m(j), \Delta p(j-1), e(k))) \right) \\ \Delta \tilde{p} = [\dots f^{-1}(\Delta u(j)) \dots]^T \quad \forall j \in J_0^{N_c-1} \\ \Delta p(j) = \Delta p(k + N_c - 1) \quad \forall j \in J_{N_c}^{N_p-1} \\ \Delta u(j) = u(j) - u_0(j) = f(p_0(j) + \Delta p(j)) - f(p_0(j)) \quad \forall j \in J_0^{N_p-1} \\ p_0(j) = f^{-1}(u_0(j)) \quad \forall j \in J_0^{N_c-1} \\ \text{and subject to the resolution of the model } (S_{LTV}). \end{array} \right. \quad (29)$$

This penalized problem can now be solved by any unconstrained optimization algorithm.

E. Control algorithm

Widely known for its robustness and convergence properties, we use of the well-known Levenberg-Marquardt's algorithm, where the argument $\Delta \tilde{p}$ is determined at each sample instant k by the iteration procedure:

$$\Delta \tilde{p}^{n+1} = \Delta \tilde{p}^n - (\nabla^2 J_{tot}^n + \lambda I)^{-1} \nabla J_{tot}^n \quad (30)$$

where ∇J_{tot}^n and $\nabla^2 J_{tot}^n$ are the criteria gradient and the criteria hessian with respect to $\Delta \tilde{p}^n$ at the iteration n . ∇J_{tot}^n is explicitly provided into the control algorithm and the classical Gauss's approximation for $\nabla^2 J_{tot}^n$ as well.

In the current MPC framework, the initial control problem (Eqs. (20) to (24)) for the RFR is therefore stated as follows:

$$\left\{ \begin{array}{l} \min_{P_{res}} J(\tilde{P}_{res}) = \sum_{j \in J_1^{N_p}} [P_{res}(j)]^2 \\ \text{where the input sequence in the future is:} \\ \tilde{P}_{res} = [P_{res}(k) \dots P_{res}(k + N_c - 1)]^T \\ \text{with constraints for the magnitude and rate of change manipulated variable:} \\ P_{res.min} \leq P_{res}(j) \leq P_{res.max} \\ \Delta P_{res.min} \leq P_{res}(j) - P_{res}(j - 1) \leq \Delta P_{res.max} \\ \text{with the process output constraint:} \\ C_g(z_{MT2}, j + 1) \leq C_{g.max} \\ \text{with the input-output relation given through the relations (1) to (13).} \end{array} \right. \quad (31)$$

From this formulation, the previous IMC-MPC strategy is developed to obtain the final penalized optimization problem (29). The use of this MPC strategy in different regimes is simulated according to three different levels of pollution at the inlet (Table 4).

A. Simulation conditions

The simulations have been realized in the following conditions:

- Concerning the spatial discretization grid for the simulated process, it has been shown to be nominally represented with 200 elements in each monoliths. It is nominal in the sense that an increase in the number of elements does not improve results anymore. The simulated process is solved by a finite volume method.
- Concerning (S_0) and (S_{LTV}) , also solved by a finite volume method, a nominal spatial discretization grid leads to a number of 60 elements in each thermal and catalytic monoliths. From the grid used for the simulated process, number of elements in the grid has therefore been divided by more than

3. Nevertheless, it does suffice to obtain good control results: it is nominal in the sense that it gives the best compromise between a good representation for the process performance (i.e. theoretically with an infinitely small grid) and a small on-line computational burden for the control algorithm (i.e. with a large grid). This is due to the use of IMC structure in the MPC strategy: like in [21], control objective are fulfilled, even if relatively large modeling errors due to the model uncertainties and model resolution are present.

- Simulations are run using a 500 MHz CPU, fortran code and ddaspg subroutine of IMSL library for the time integration.

- The temperature $T_{g,\text{inlet}}(t)$ of the gas at the inlet of the reactor as well as its flow rate $Q_g(t)$ are assumed constant and measured:

$$\begin{cases} T_{g,\text{inlet}}(t) = 20^\circ C \\ Q_g(t) = 100 \text{ m}^3.h^{-1} \end{cases} \quad (32)$$

and u_g is the gas velocity in the canals.

- A preheating period is necessary before using the reactor with polluted gas. During this period, the catalytic elements temperature increases such that the reaction can be possible. This preheating is done in the following conditions:

$$\begin{cases} N_{cycles} = 300 (-) \\ P_{res}(t) = 520 \text{ W} \\ C_{g,\text{inlet}}(t) = 0 \text{ mol.m}^{-3} \\ T_g(z, 0) = 20^\circ C \\ C_g(z, 0) = 0 \text{ mol.m}^{-3} \\ T_s(z, 0) = 20^\circ C \\ C_s(z, 0) = 0 \text{ mol.m}^{-3} \end{cases} \quad (33)$$

- After trial error tests, the model linearization is done around the nonlinear behavior obtained with:

$$\begin{cases} P_{res,0}(t) = 500 \text{ W} \\ C_{g,inlet,0}(t) = 2 \cdot 10^{-3} \text{ mol.m}^{-3} \end{cases} \quad (34)$$

- Constraints bounds are:

$$\begin{cases} P_{res,max} = 3000 \text{ W} \\ P_{res,min} = 0 \text{ W} \\ \Delta P_{res,max} = +1500 \text{ W.s}^{-1} \\ \Delta P_{res,min} = -1500 \text{ W.s}^{-1} \\ C_{g,max} = 4.7 \cdot 10^{-4} \text{ mol.m}^{-3} \end{cases} \quad (35)$$

- For the output constraints (19), the length of the time window T is 20 *min*.
- The maximum temperature along the reactor must not exceed 650°C.
- In this initial approach, the sample rate T_e value is half of the cycle period (round trip) T_{cycle} value:

$$\begin{cases} T_{cycle} = 20s \\ T_e = 0.5 T_{cycle} \end{cases} \quad (36)$$

The gas properties are assumed to be measured. Since the gas concentration has a stochastic behavior and has a strong influence over the prediction of the output behavior and therefore over the control results, a one step-ahead prediction is employed. In the meantime, this automatically tunes the control horizon N_c to 1. Then, the MPC algorithm aims to minimize the effect of the level of input concentration over the process output as fast as possible.

Remark VI.1: To see a smooth trend of the electrical power fed into the central zone, the mean value calculated since the beginning of the run, including the warm-up period, is depicted instead of the value found at each time. In each case, the mean electrical power fed to the central zone is time-decreasing since the initial warm-up is done at 520 W and that after that, the value of electrical power is less important.

Remark VI.2: For all the output concentrations depicted, the discontinuity that occurs at 1200s is due to the initial memorisation needed to calculate the constraint (19).

B. Simulation results

Finally, these runs allow to see three different regimes for the use of the reactor:

- In the low level case, the heat generated during the exothermic catalytic reaction of the pollutant is not enough for an autonomous use of the reactor. Therefore, an external source of energy is needed and electrical power is fed into the reactor (Fig. 6) to achieve the depollution objective described by the output constraint (19) (Fig. 7). The control objective is achieved since the maximum threshold of pollution is never exceeded;
- In the medium level case, as expected, about 1% of the full capacity of electrical supply need to be used (Fig. 8). In this case, the concentration of pollutant becomes sufficiently high such that the heat generated during the reaction allows to be near a particular regime: the autothermic regime where no external source of energy is needed to satisfy the output constraint (Fig. 9);
- In the high level case, as expected, the autothermic regime is reached: Fig. 10 shows that no external source of energy is needed and that the output constraint is amply checked (Fig. 11). The drawback is that the maximum temperature in the reactor exceeds the maximum admissible limit (Fig. 12): the catalytic elements are destroyed and the reactor is no longer efficient. Since this phenomenon has to be avoided, this clearly underlines the necessity to add a cooling system in order to operate the reactor in any of the three proposed different regimes. The related MIMO system control is actually under study.

In the meantime, one can notice the sensitivity of the output concentration (Fig. 13) versus the electrical power (Fig. 14) from two runs in the low level case with the same inlet gas concentration but changing the nominal grid to an alternate grid for the model. It shows that, by reducing the consumption of electrical energy by 50 W only, the output concentration increases by 200 % whereas

the output constraint is still satisfied. Regarding the range of 3000 W that can be used for the manipulated variable, it indicates that a very tight control is achieved and it underlines the effect of tuning the number of elements in the grid needed to solve the model.

VII. CONCLUSIONS AND PERSPECTIVES

This paper deals with the model predictive control strategy of a catalytic reverse flow reactor. This process is used to decrease noxious VOC amount in gas released in the atmosphere. The complexity of this process includes distributed aspect, nonlinear dynamic behavior and periodic reversing of the circulation of gas. Until now, even if the initial control problem stated as a temperature regulation is solved, it gives bad overall performance: overconsumption of electrical power must be avoided. To optimize the control of this reactor, an IMC-MPC framework has been developed. It is based on the first-principles nonlinear distributed parameter model obtained from heat and mass balances detailed in the paper. Regarding numerical issues, even if a relatively large-scale model needs to be solved in the MPC strategy with a small sample time of 10s, the on-line implementation is possible. Simulations allow to check the efficiency of this approach and to give some guidelines for current directions of research. New advances are currently being studied for new problems: control of the MIMO system that includes the cooling system and development of a model-based observer to estimate the inlet concentration that aims to replace a costly sensor.

REFERENCES

- [1] Y.S. MATROS AND G.A. BUNIMOVICH, "Reverse-flow Operation in Fixed Bed Catalytic Reactors," *Cat. Rev.-Sci. Eng.*, vol. 38, no. 1, pp. 1-68, 1996.
- [2] U. NIEKEN, G. KOLIOS AND G. EIGENBERGER, "Control of the Ignited Steady State in Autothermal Fixed-bed Reactors for Catalytic Combustion," *Chem. Eng. Sci.*, vol. 49, no. 24B, pp. 5507-5518, 1994.
- [3] U. NIEKEN, G. KOLIOS AND G. EIGENBERGER, "Limiting Cases and Approximate Solutions for Fixed-bed Reactors with Periodic Flow Reversal," *AIChE J.*, vol. 41, no. 8, pp. 1915-1924, 1995.
- [4] T.N. HAYNES, C. GEORGAKIS AND H.S. CARAM, "The Design of Reverse Flow Reactors for Catalytic Combustion Systems," *Chem. Eng. Sci.*, vol. 50, pp. 401-416, 1995.

- [5] B. VAN DE BELD AND K.R. WESTERTERP, "Air Purification by Catalytic Oxidation in a Reactor with Periodic Flow Reversal," *Chem. Eng. Technol.*, vol. 17, pp. 217–226, 1994.
- [6] F. CUNILL, L. VAN DE BELD AND K.R. WESTERTERP, "Catalytic Combustion of Very Lean Mixtures in a Reverse Flow Reactor using an Internal Electrical Heater," *Ind. Eng. Chem. Res.*, vol. 36, pp. 4198–4206, 1997.
- [7] K. RAMDANI, R. PONTIER AND D. SCHWEICH, "Reverse Flow Reactor at Short Switching Periods for VOC Combustion," *Chem. Eng. Sci.*, vol. 56, pp. 1531–1539, 2001.
- [8] BUDMAN H., KZYONSEK M., SILVERSTON P., "Control of a Nonadiabatic Packed Bed Reactor under Periodic Flow Reversal," *The Canadian Journal of Chem. Eng.*, vol. 74, pp. 751–759, 1996.
- [9] K. RAMDANI, *Le Réacteur à Inversion de Flux pour la Destruction de Composés Organiques Volatils. Modèles, Expériences et Dynamique*, Ph.D. thesis, Université Claude Bernard Lyon 1, 2000.
- [10] BARBU V., *Analysis and Control of Nonlinear Infinite Dimensional Systems*, Academic Press Inc., 1993.
- [11] PAZY A., *Semigroups of linear Operators and Applications to Partial Differential Equations*, Springer Verlag New-York, 1983.
- [12] M. CITTADINI, M. VANNI, A.A. BARRESI AND G. BALDI, "Simplified Procedure for Design of Catalytic Combustors with Periodic Flow Reversal," *Chem. Eng. Process.*, vol. 40, no. 3, pp. 255–262, 2001.
- [13] HENSON, M.A., "Nonlinear Model Predictive Control: Current Status and Future Directions," *Comp. & Chem. Eng.*, vol. 23, no. 2, pp. 187–202, 1998.
- [14] MORARI, M., & LEE, J.H., "Model Predictive Control: Past, Present and Future," *Comp. & Chem. Eng.*, vol. 23, no. 4-5, pp. 667–682, 1999.
- [15] D.Q. MAYNE, J.B. RAWLINGS, C.V RAO AND P.O.M. SOKAERT, "Constrained Model Predictive Control: Stability and Optimality," *Automatica*, vol. 36, no. 6, pp. 789–814, 2000.
- [16] RAWLINGS, J.B., "Tutorial Overview of Model Predictive Control," *IEEE Control Systems*, vol. 20, no. 3, pp. 38–52, 2000.
- [17] MORARI M., ZAFIRIOU E., *Robust Process Control*, Prentice-Hall, Englewood Cliffs, New Jersey, 1989.
- [18] TOURÉ Y., JOSSERAND L., "An Extension of IMC to Boundary Control of Distributed Parameter Systems," in *IEEE International Conference on Systems, Man and Cybernetics-CCS*, Orlando, 1997, vol. 3, pp. 2426–2431.
- [19] MARQUIS P., BROUSTAIL J.P., "SMOC, a Bridge between State Space and Model Predictive Controllers : Application to the Automation of a Hydrotreating Unit," in *Proc. of the 1988 IFAC Workshop on Model Based Process Control*, McAvoy T.J. Arkun Y. Zafriou E., Ed., Oxford, 1988, pp. 37–43, Pergamon Press.
- [20] R. FLETCHER, *Practical Methods of Optimization*, John Wiley and Sons, 1987.
- [21] M.C LARABI, P. DUFOUR, P. LAURENT AND Y. TOURÉ, "Predictive Control of a Nonlinear Distributed Parameter System: Real Time Control of a Painting Film Drying Process," in *Proc. MTNS*, Perpignan, 2000, p. Paper B167.

VIII. LIST OF TABLES AND FIGURES

Reference	Label
Table 1	List of tables and figures
Table 2	Parameters value for the cordierite and the gas
Table 3	Geometric data for the reactor
Table 4	Levels of pollutant at the inlet
Figure 1	Principle scheme for the catalytic reverse flow reactor
Figure 2	Monolith section
Figure 3	Spatial discretization in the reactor
Figure 4	General IMC-MPC structure
Figure 5	General linearized IMC-MPC structure
Figure 6	Mean electrical power for low concentration of pollutant at the inlet
Figure 7	Mean concentration of pollutant at the outlet for low concentration of pollutant at the inlet
Figure 8	Mean electrical power for medium concentration of pollutant at the inlet
Figure 9	Mean concentration of pollutant at the outlet for medium concentration of pollutant at the inlet
Figure 10	Mean electrical power for high concentration of pollutant at the inlet
Figure 11	Mean concentration of pollutant at the outlet for high concentration of pollutant at the inlet
Figure 12	Maximum temperature in the process for high concentration of pollutant at the inlet
Figure 13	Mean pollutant concentration at the outlet: nominal (solid) and not nominal (dotted) cases
Figure 14	Mean electrical power: nominal (solid) and not nominal (dotted) cases

Table 1.

Signification	Name	Value	Unit
Solid density in the thermic elements	ρ_{st}	2500	$kg.m^{-3}$
Solid density in the catalytic elements	ρ_{sc}	4000	$kg.m^{-3}$
Gas density	ρ_g	1.2	$kg.m^{-3}$
Thermal capacity for the solid	c_{p_s}	850	$J.kg^{-1}.K^{-1}$
Thermal capacity for the gas	c_{p_g}	1030	$J.kg^{-1}.K^{-1}$
Thermal conductivity coefficient	λ	1.5	$W.m^{-1}.K^{-1}$
Heat transfer coefficient	h	32	$W.m^{-2}.K^{-1}$
Kinetic constant of reaction	k^∞	300	$m.s^{-1}$
Mass transfer coefficient	k_d	0.11	$m.s^{-1}$
Reaction activation energy	E_a	$4.2 \cdot 10^4$	$J.mol^{-1}$
Reaction enthalpy	$(-\Delta H_r)$	$4.6 \cdot 10^6$	$J.mol^{-1}$
Perfect gas constant	R	8.314	$J.mol^{-1}.K^{-1}$

Table 2.

Signification	Name	Value	Unit
Empty volume / total volume ratio	ε	70%	(-)
Length of a thermal monolith	L_{MT}	0.375	m
Length of a catalytic monolith	L_{MC}	0.075	m
Central zone length	L_{ZC}	0.60	m
Canal diameter	d_h	0.00109	m
Number of canals	nb_c	13225	(-)
Central zone section	S	0.0225	m^2
Specific surface area per unit volume	a_c	$\frac{4\varepsilon}{d_h}$	$m^2.m^{-3}$

Table 3.

Regime	Input concentration ($mol.m^{-3}$)
Low level	$1 \cdot 10^{-3} < . < 3 \cdot 10^{-3}$
Medium level	$4 \cdot 10^{-3} < . < 6 \cdot 10^{-3}$
High level	$16 \cdot 10^{-3} < . < 18 \cdot 10^{-3}$

Table 4.

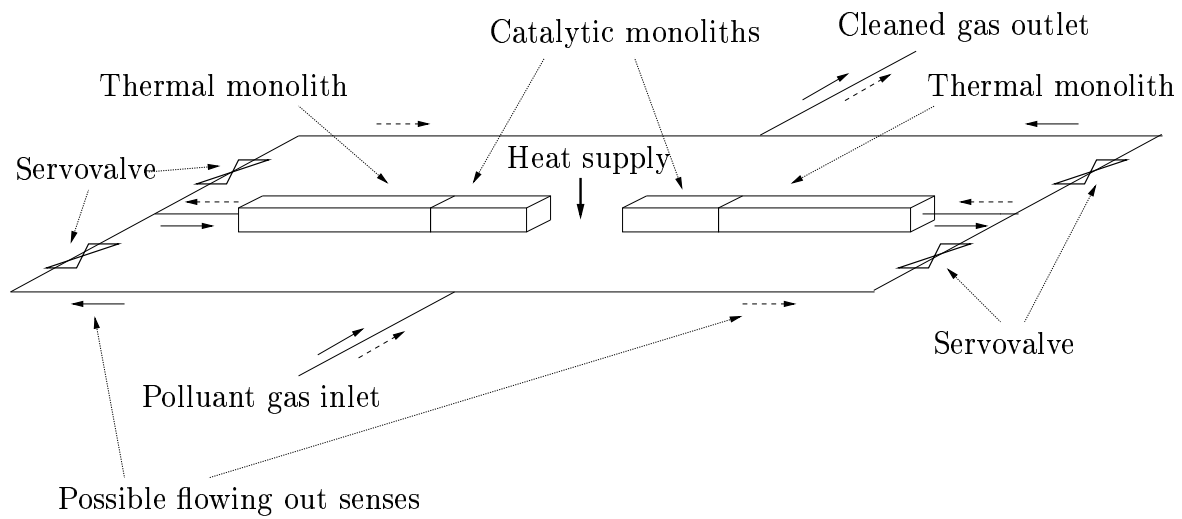


Fig. 1.

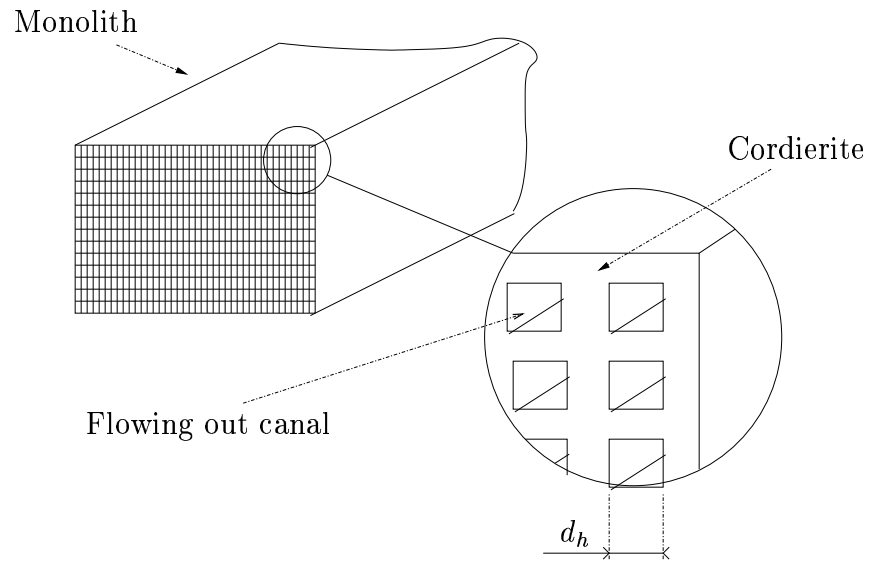


Fig. 2.

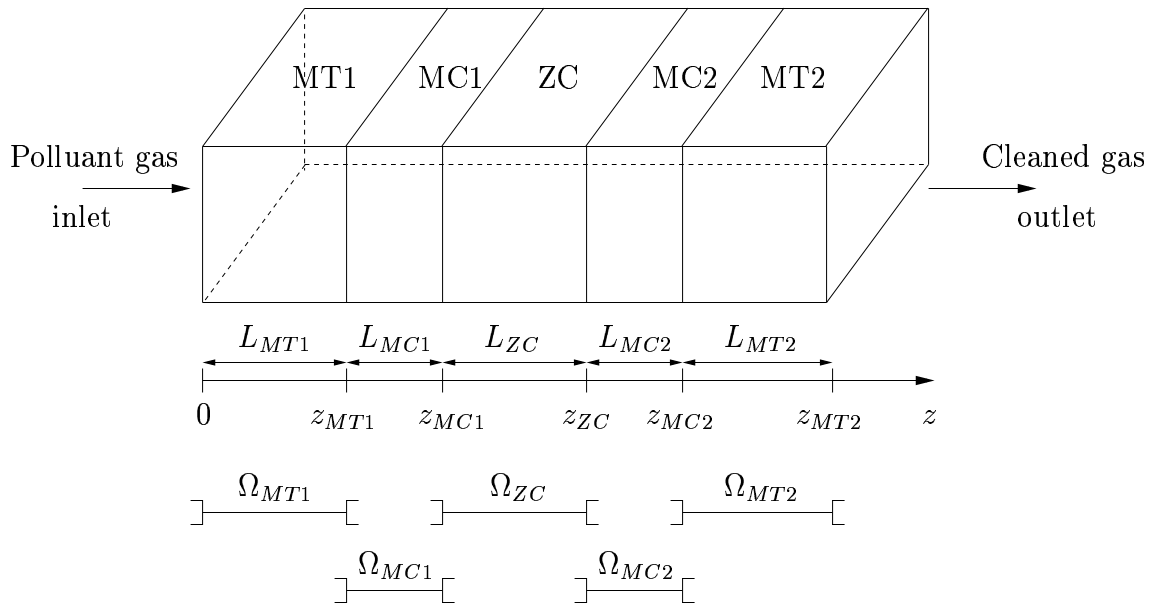


Fig. 3.

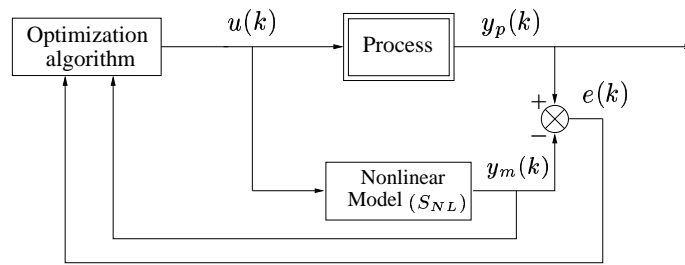


Fig. 4.

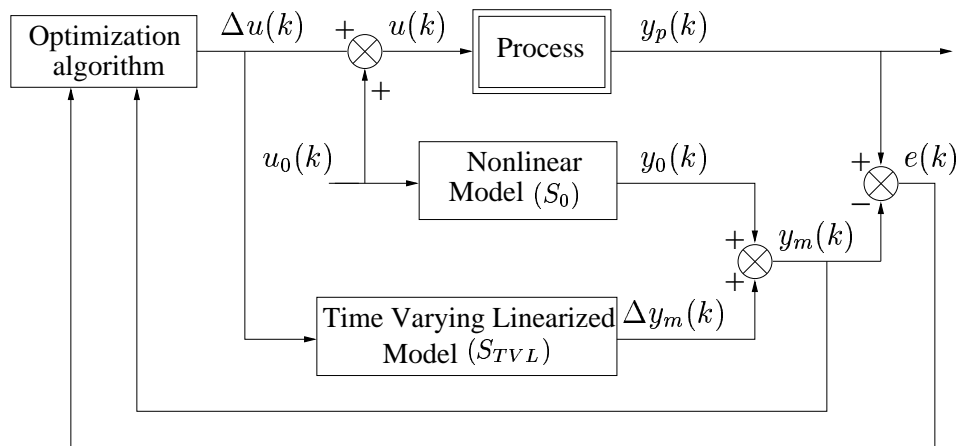


Fig. 5.

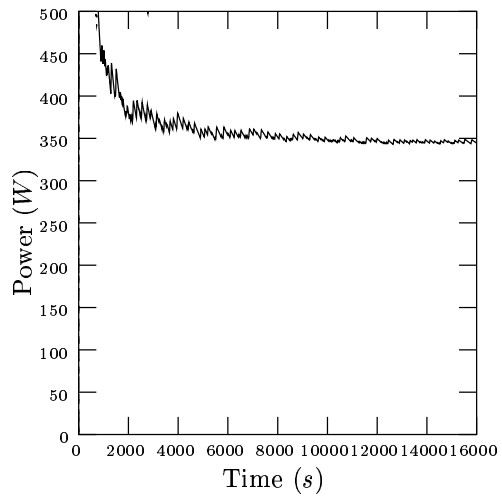


Fig. 6.

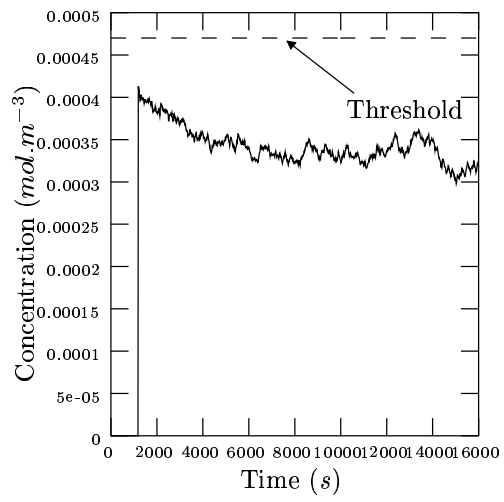


Fig. 7.

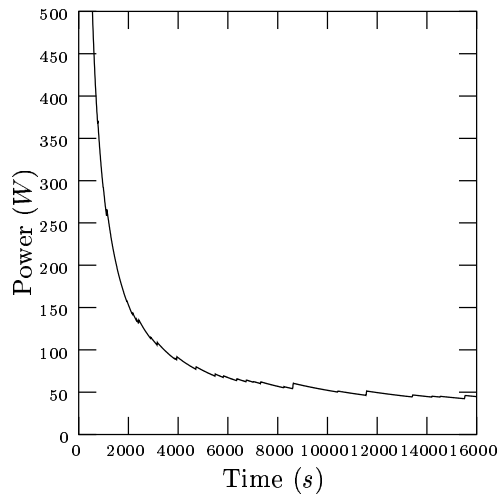


Fig. 8.

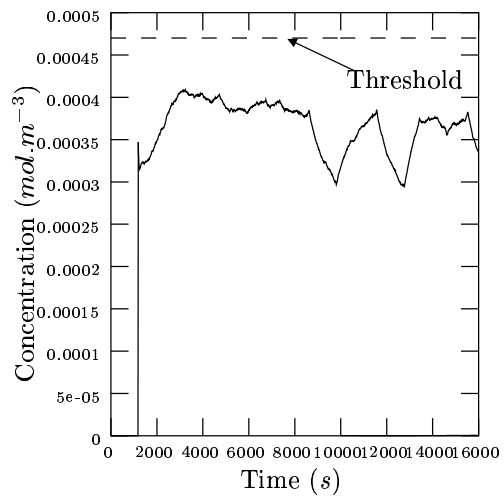


Fig. 9.

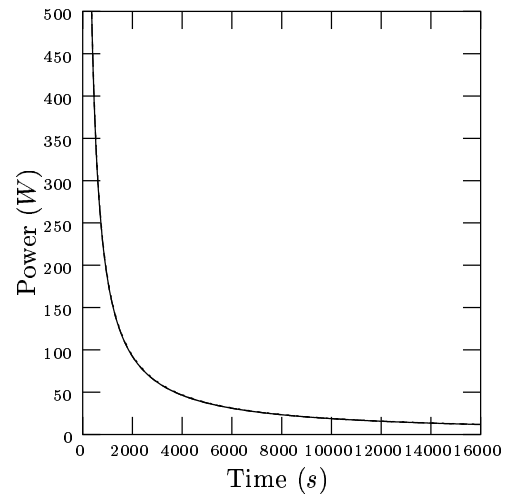


Fig. 10.

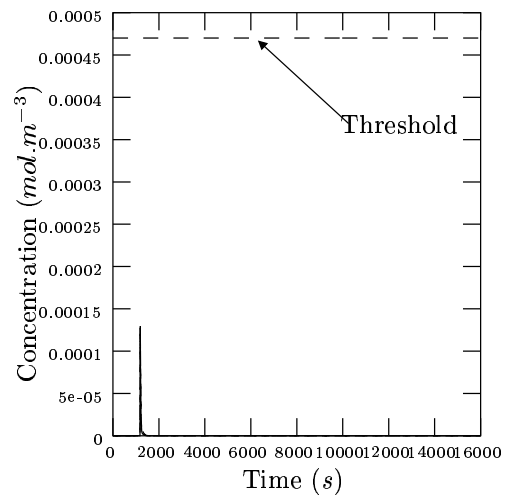


Fig. 11.

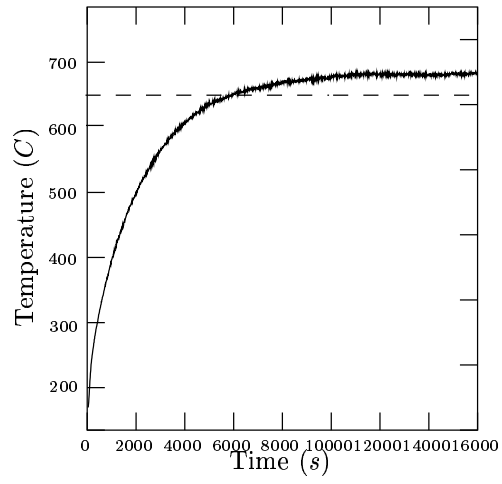


Fig. 12.

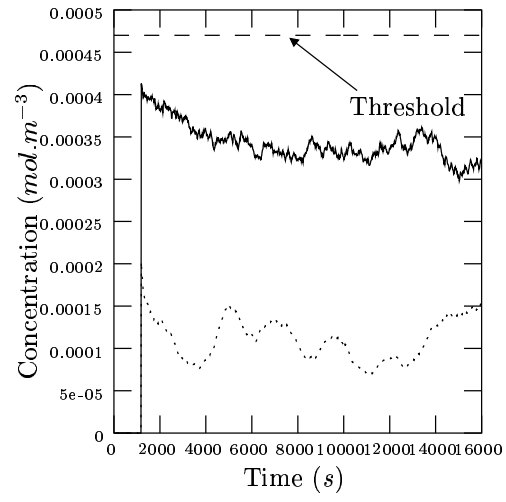


Fig. 13.

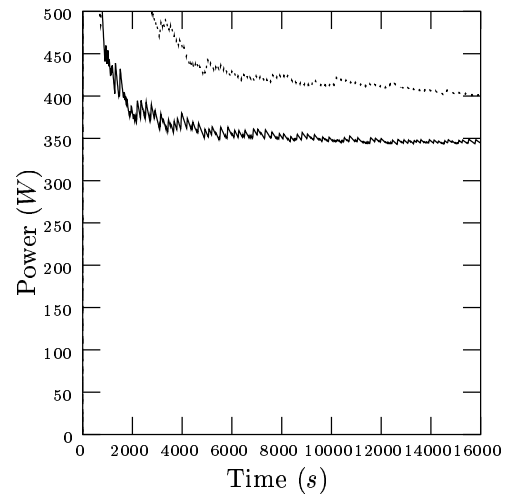


Fig. 14.